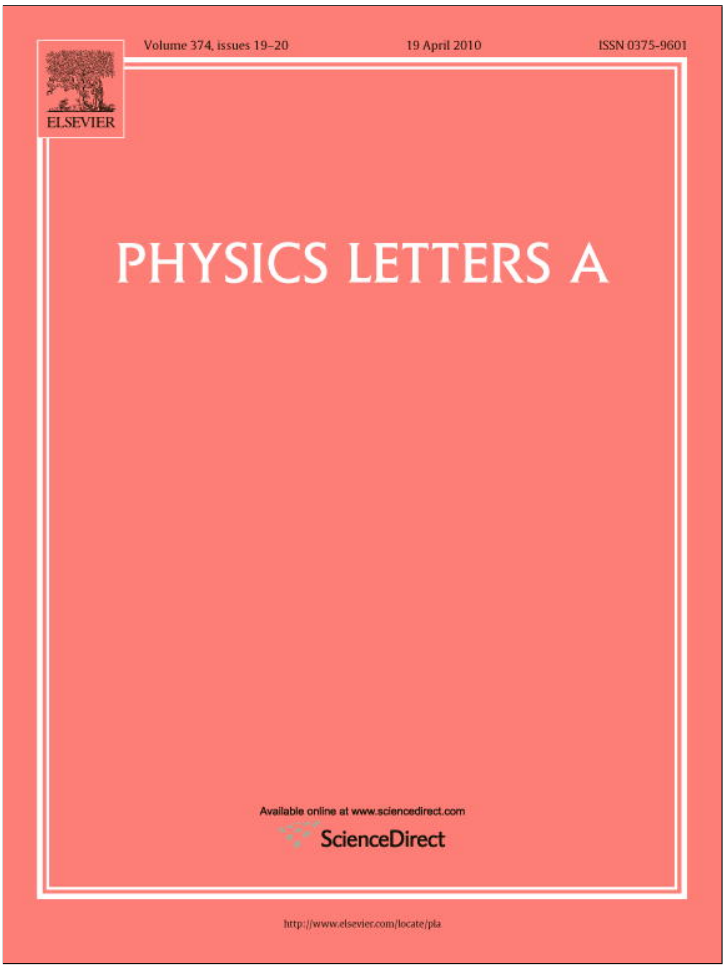

Physics Letters A 374 (2010) 2053–2057

Contents lists available at ScienceDirect

Physics Letters A

www.elsevier.com/locate/pla

The transverse elasticity of bilayer graphene

F. Scarpa [a,*], S. Adhikari [b], R. Chowdhury [b]

[a] Advanced Composites Centre for Innovation and Science, University of Bristol, BS8 1TR Bristol, UK
[b] Multidisciplinary Nanotechnology Centre, Swansea University, SA2 8PP Swansea, UK

ARTICLE INFO

Article history:
Received 30 December 2009
Received in revised form 22 February 2010
Accepted 24 February 2010
Available online 26 February 2010
Communicated by R. Wu

Keywords:
Bilayer graphene
Mechanics
Stiffness
Shear deformation

ABSTRACT

We demonstrate that the mechanical behaviour of bilayer graphene can be predicted using a first order deformation approach typical of sandwich structures. The mechanical transverse deformation of bilayer graphene under central loading is simulated using a mixed atomistic continuum – Finite Element technique, and the results post-processed using a First Order Sandwich Structures (FOSS) deformation approach. The proposed technique provides good agreement with experimental and theoretical data available in open literature.

1. Introduction

Bilayer graphene has been proposed as the only semiconductor to produce insulating state and switch-off electrical conduction [1,2]. Another unusual property of this nanomaterial is the presence of two structural domains at 180° when grown on SiC substrate, showing a "shifted stacking" of the layers due to lattice mismatch induced by the roughness of the silicon carbide [3]. Low-frequency electrical resistance fluctuations in bilayer and multilayer graphene has been studied in [4,5]. Electron diffraction has also allowed to identify significant roughness in suspended bilayer graphene membranes, although with a lower degree than single layer graphene sheets [6]. AFM techniques have been also applied to suspended multilayer graphene sheets, showing a measured Young's modulus of 0.5 TPa [7], half of the classical value accepted in literature from simulations and experimental results on single layer graphene structures [8–11]. The peculiar structure of the bilayer graphene could explain the above discrepancy.

Bilayer graphene is composed by two single layers of graphene, interacting each other with Van der Walls forces, which can be expressed in terms of Lennard-Jones (LJ) potentials. From a geometric perspective, there is a significant similarity between bilayer graphene and sandwich panels or beams. Structural sandwich structures are made by two face skins embedding a core material. According to the first-order shear deformation theory [12], the face skins bear the flexural stiffness of the system, while the shear stiffness of the core provides the added transverse deformation of the panel, when subjected to concentrated or distributed loads. As an initial approximation, one can presume that the single sheets of bilayer graphene could be assimilated to the plates of the face skins, while the interlayer Lennard-Jones potential can be thought as the "core" of the nanostructure. Several authors have considered a structural modelling of multilayer graphene, both in terms of analytical and molecular simulations [13–16], and equivalent continuum modelling of the plates as structural shells, while the LJ potentials have been represented as equivalent connecting springs [17]. The use of an equivalent first-order sandwich structure (FOSS) theory to model the mechanical behaviour of bilayer graphene would have some appealing features. According to the FOSS approach [12,18], it is possible to decouple the elasticity of the upper and lower plates of the sandwich from the one of the core, therefore determining the contributions from the single components of the nanostructure to the overall mechanics of the bilayer. Secondly, the FOSS approach would also provide a framework for an experimental technique to measure the mechanical properties of bilayer graphene, using the formulations used in mechanical testing of sandwich components [18].

This Letter aims at exploring the feasibility of using the FOSS theory on bilayer graphene, using the simulations related to a 3-point loading on bilayer graphene nanostructures as "experimental data". The graphene nanostructures are represented by an equivalent atomistic-continuum Finite Element (FE) representation of the C–C bonds [19] and LJ potentials. The method developed by some of the present authors and applied to single layer graphene sheets [20], is based on a representation of the covalent carbon bonds for the graphene with deep shear beams with bending and axial deformation, and equivalent mechanical properties determined

* Corresponding author. Tel.: +44 (0)117 3315306; fax: +44 (0)117 9272771.
E-mail addresses: f.scarpa@bristol.ac.uk (F. Scarpa), S.Adhikari@swansea.ac.uk (S. Adhikari), R.Chowdhury@swansea.ac.uk (R. Chowdhury).

0375-9601/$ – see front matter
doi:10.1016/j.physleta.2010.02.063

by the minimisation of the total potential energy under specific loading and boundary conditions. In other terms, the mechanical characteristics (thickness, distribution of the bond lengths) are functions of the loading and constraints applied to the nanostructure. This approach is consistent with the large spread of thickness values observed for CNTs and graphene (the "Yakobson's paradox" [21]), as well as the different C–C bond equilibrium lengths observed in graphene sheets under different loading conditions [22,23]. To account for the effects of the LJ potential between the single graphene layers, we have developed an equivalent nonlinear spring Finite Element, reproducing the axial deformations and cut-off properties of the potential as idealised by Girifalco et al. [24]. The atomistic-continuum FE models of the bilayer graphene have been subjected to 3-point bending loading conditions – i.e., simply supported at the two ends, with a central concentrated loading. The results of the numerical simulations have been post processed with the FOSS theory, and the equivalent bending and shear stiffness of the graphene layers and LJ potential respectively compared with existing data from open literature. We will show that the FOSS approach can reproduce the bending stiffness provided by the single graphene sheets, while the transverse shear can be approximated only for deflections up to 18%–20% of length from the supports. However, the flexural modulus identified with this technique yields values close to the 0.5 TPa measured experimentally in suspended multilayer graphene, as well as membrane stiffnesses in good agreement with the ones calculated with *ab initio* and MD techniques in graphene sheets.

2. Methodology

2.1. C–C bonds modelling

We follow the approach from [19,20] to model the covalent carbon–carbon bond in single layer graphene. The carbon–carbon sp^2 bonds can be considered as equivalent beams having axial, out-of-plane and in-plane rotational deformation mechanisms. The harmonic potential associated to the C–C bond can be expressed as:

$$\begin{aligned}
&\frac{k_r}{2}(\delta r)^2 = \frac{EA}{2L}(\delta r)^2 \\
&\frac{k_\tau}{2}(\delta\varphi)^2 = \frac{GJ}{2L}(\delta\varphi)^2 \\
&\frac{k_\theta}{2}(\delta\theta)^2 = \frac{EI}{2L}\frac{4+\Phi}{1+\Phi}(\delta\theta)^2
\end{aligned} \tag{1}$$

The first row of (1) corresponds to the equivalence between stretching and axial deformation mechanism (with E being the equivalent Young's modulus), while the second one equates the torsional deformation of the C–C bond with the pure shear deflection of the structural beam associated to an equivalent shear modulus G. The term equating the in-plane rotation of the C–C bond (third row of (1)) is equated to a bending strain energy related to a deep shear beam model, to take into account the shear deformation of the cross section. The shear correction term becomes necessary when considering beams with aspect ratio lower than 10 [25]. For circular cross sections, the shear deformation constant can be expressed as [20]:

$$\Phi = \frac{12EI}{GA_sL^2} \tag{2}$$

In (2), $A_s = A/F_s$ is the reduced cross section of the beam by the shear correction term F_s [26]:

$$F_s = \frac{6+12\nu+6\nu^2}{7+12\nu+4\nu^2} \tag{3}$$

The insertion of (2) and (3) in (1) leads to an nonlinear relation between the thickness d and the Poisson's ratio ν of the equivalent beam [20]:

$$k_\theta = \frac{k_r d^2}{16}\frac{4A+B}{A+B} \tag{4}$$

Where:

$$A = 112L^2k_\tau + 192L^2k_\tau\nu + 64L^2k_\tau\nu^2 \tag{5}$$

$$B = 9k_rd^2 + 18k_rd^4\nu + 9k_rd^4\nu^2 \tag{6}$$

The values for the force constants for the AMBER model are $k_r = 6.52\times10^{-7}$ N mm^{-1}, $k_\theta = 8.76\times10^{-10}$ N nm rad^{-2}, and $k_\tau = 2.78\times10^{-10}$ N nm^{-1} rad^{-2} [27]. For the linearised version of the Morse potential, we adopt $k_r = 8.74\times10^{-7}$ N mm^{-1}, $k_\theta = 9.00\times10^{-10}$ N nm rad^{-2} and $k_\tau = 2.78\times10^{-10}$ N nm^{-1} rad^{-2} [20]. The equivalent mechanical properties of the C–C bond can be determined performing a nonlinear optimisation of (1) using a Marquardt algorithm.

2.2. Lennard-Jones potential

The equivalent axial force related to the LJ potential between pair of atoms (i, j) belonging to different graphite layers can be expressed as:

$$F_{ij} = \frac{\partial V_{ij}}{\partial r} \tag{7}$$

Where r is the deformation along the distance **ij** between the atoms pair. Using the formulation from Girifalco et al. [24], the force exerted between the two atoms can be expressed as:

$$F_{ij} = -12\epsilon\left[\left(\frac{r_{min}}{y}\right)^{13} - \left(\frac{r_{min}}{y}\right)^{7}\right] \tag{8}$$

Where $y = r_{min} + \delta r$, δr being the deformation along **ij**. The minimum (cut-off) distance r_{min} (in Å) is equal to $2^{\frac{1}{6}}\sigma$, where $\sigma = (A/B)^{1/6}$. The attractive and repulsive constants B and A for the interlayer graphitic potential are 24.3×10^3 eV × Å^{12} and 15.4 eV × Å^6 respectively. The term ϵ is equal to $B^2/(4A)$.

The upper and lower graphene sheets are modelled using the deep shear (Timoshenko) Finite Element beams [28,29], where the nodes represent the atoms. Each atom of the bond laying in one layer is connected to the nearest and near neighbour in the opposite plane using a nonlinear spring element with stiffness matrix updated through a Newton–Raphson scheme at selected points of the force displacement curve (8). The bilayer graphene (Fig. 1) is simply supported (SS) at the ends (displacements, and out-of-plane rotations constrained), while a central loading is applied along the nodes (atoms) on the middle plane of the upper single layer graphene. The SS boundary conditions have been applied to conform to the determination of the flexural stiffness and equivalent core shear modulus in classical FOSS measurements [12]. We observe, however, that the mechanical properties obtained using homogenisation techniques are affected, especially at nanoscale (and for graphene), by the specific boundary conditions used and scale effects given by the relative length between lattice dimensions and overall nanostructure [30]. All the simulations were carried out considering room temperature conditions ($T = 300$ K), and no in-plane pre-tension applied. In this way, only the membrane and flexural properties on the bilayer alone were considered, with no induced stiffening effect given by other membrane states. The equivalent mechanical properties of the C–C bonds (from Eqs. (1), (4)) are computed after the minimisation of the total potential energy associated to the specific loading and boundary conditions. Following [20], a two-step nonlinear optimisation is performed,

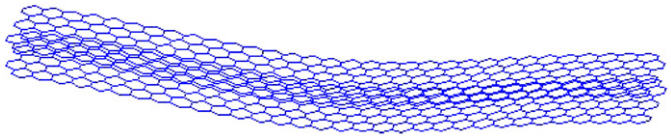

Fig. 1. Bilayer graphene (length 7.99 nm, width 1.35 nm, interlayer distance 0.34 nm) under 3-point bending loading.

using first a zero-order optimisation routine, and then a steepest-descent first-order technique to identify the global minima of the potential energy. The simulation technique has been applied to 3 bilayer graphene, with overall length a of 7.99 nm and different aspect ratios (8.64, 5.91, 3.05). The interlayer distance h was considered equal to 0.34 nm [24,1]. Both AMBER and linearised Morse potential force models were considered for each bilayer graphene model.

3. Results and discussions

3.1. Thickness and equilibrium lengths

Table 1 shows the distribution of the thickness and equilibrium lengths belonging to the upper and lower graphene sheets after the minimisation of the potential energy. One significant aspect to notice is the different thickness amongst the upper and lower graphene sheets, with the highest thickness values corresponding to the single graphene layer directly loaded. The average values at equilibrium oscillate between 0.138 nm and 0.142 nm. Reddy et al. [22] have observed C–C bond lengths distributions between 0.139 nm (in the middle of the graphene), to 0.147 nm at the edges, for the case of pure uni-axial in-plane tensile loading. Although larger bond lengths ranges are possible when Stone–Walls defects are considered [31], the majority of the values we identify are within 0.141 nm and 0.142 nm, well close to the standard equilibrium length for the C–C bonds in carbon nanotubes and graphene [32]. While the distribution of the bond lengths seems not affected by the force model used, the values of the thickness vary whether the AMBER or Morse models are used. For the AMBER case, the thickness vary between 0.111 nm and 0.116 nm, with lower values (0.103 nm and 0.109 nm) for the linearised Morse potential. These values are consistent with the 0.120 nm identified by Sun et al. in CNTs [33], and the 0.137 nm from Hemmasizadeh et al. [8] for the bending of a single layer graphene. Batra and Gupta [34] identify thickness of the order of 0.1 nm for single wall carbon nanotubes undergoing resonant behaviour. Lower thickness values are also identified in open literature (0.057 nm [35], 0.074 nm [36], 0.084 nm [37,20]), but they are all related to single layer graphene sheets under uni-axial in-plane loading only.

3.2. Stiffness of the bilayer graphene

The transverse displacement δ at location x of a sandwich beam under concentrated transverse central loading F can be expressed as [12,18]:

$$\delta = \delta_b + \delta_s = \frac{Fx^3}{48D} + \frac{Fx}{4U} \tag{9}$$

Where δ_b and δ_s are the transverse displacements due to bending of the single graphene layers and the shear of the Lennard-Jones potentials. In (9), the equivalent shear stiffness G of the core is provided through the load bearing cross section U. For uneven face skin thickness d_u and d_l, the flexural stiffness D per unit width is expressed as [12]:

$$D = E_f\left[\left(\bar{h}^2\frac{d_u d_l}{d_u + d_l}\right) + \frac{1}{12}\left(d_u^3 + d_l^3\right)\right] \tag{10}$$

Table 1
Thickness and equilibrium lengths of the bilayer graphene after minimisation of the total potential energy. The subscripts l and u refer to the lower and upper sheets of the bilayer graphene.

a [nm]	b [nm]	d_l [nm]	d_u [nm]	L_l [nm]	L_u [nm]	Force model
7.99	0.92	0.111	0.116	0.142	0.141	AMBER
7.99	1.35	0.112	0.112	0.138	0.141	AMBER
7.99	2.63	0.111	0.116	0.143	0.142	AMBER
7.99	0.92	0.106	0.107	0.142	0.142	Morse
7.99	1.35	0.103	0.109	0.142	0.141	Morse
7.99	2.63	0.108	0.108	0.142	0.142	Morse

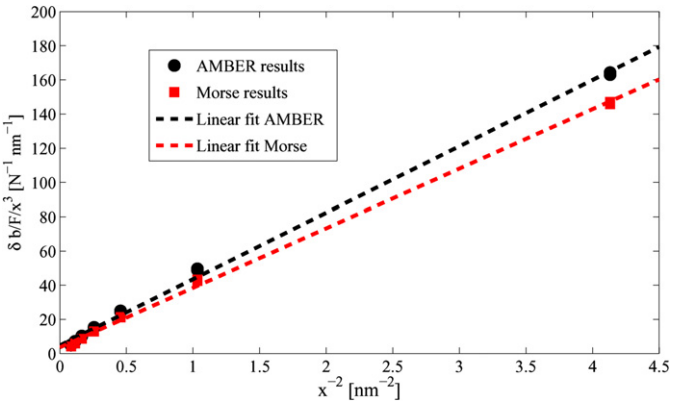

Fig. 2. Total displacements of the bilayer from Eq. (12) with linear LS fitting.

Where E_f is the flexural modulus of single layer graphene sheets, while $\bar{h} = h + (d_u + d_l)/2$, h being the atomic interlayer distance (0.34 nm). The shear stiffness U of the core (LJ potential) is formulated as [12]:

$$U = G_{LJ}\bar{h} \tag{11}$$

Where G_{LJ} is the equivalent transverse shear provided by the Lennard-Jones potential. Eq. (9) can be conveniently recast to express linear fits to identify the effective flexural stiffness and transverse shear of the bilayer graphene in the following way:

$$\frac{\delta b}{Fx^3} = \frac{1}{48D} + \frac{b}{4U}\frac{1}{x^2} \tag{12}$$

$$\frac{\delta b}{Fx} = \frac{b}{4U} + \frac{x^2}{48D} \tag{13}$$

The linear polynomial fit for Eq. (12) and AMBER force model, with a $R^2 = 0.99$ and confidence interval of 95% provides the following approximation: $\delta b/F/x^3 = 4.711 + 38.8(1/x^2)$. For the linearised Morse potential, the linear fit becomes $\delta b/F/x^3 = 3.627 + 34.8(1/x^2)$, always with a R^2 of 0.99 (Fig. 2). For the shear-induced displacement in Eq. (13), the assumption for the transverse simple shear deformation seems no more valid. On the contrary, the curve assumes an exponential fit of the type: $\delta b/F/x = c_1\exp(c_2x^2) + c_3\exp(c_4x^2)$ (Fig. 3). For the linearised Morse potential, the values of the coefficients are $c_1 = 61.35$, $c_2 = -0.0175$, $c_3 = -27.74$ and $c_4 = -0.378$. For the AMBER force model, the values of the coefficients are the following: $c_1 = 71.09$, $c_2 = -0.016$, $c_3 = -33.84$ and $c_4 = -0.367$. All the fitted curves showed a R^2 of 0.98. The bilayer graphene seems to feature the equivalent sandwich structure behaviour (i.e., linearity of the normalised displacement versus x^2) up to 20% of the width a of the bilayer from the supports (Fig. 3). For that case, the linear behaviour of Eq. (13) is expressed by an approximation of the type $\delta b/F/x \approx b_1 + b_2x^2$, where $b_1 = 38.95$ and $b_2 = 7.33$ for the AMBER force model. The linearised Morse potential case fits in Least Squares the approximation with $b_1 = 34.89$ and $b_2 = 5.67$. It is worth noticing that

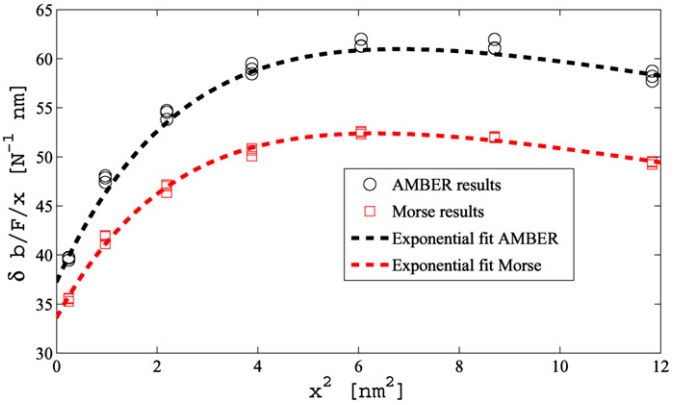

Fig. 3. Total displacement $\delta b/F/x$ versus x^2 with exponential LS fits for AMBER and linearised Morse potential results.

Table 2
Flexural modulus and equivalent shear of the bilayer graphene sheets using Eqs. (10) and (11) – unsymmetric thickness of the single graphene layers.

Dimensions [nm × nm]	E_f [TPa]	G_{LJ} [TPa]	Force model
7.99 × 0.92	0.371	0.0142	AMBER
7.99 × 1.35	0.379	0.0143	AMBER
7.99 × 2.63	0.371	0.0143	AMBER
7.99 × 0.92	0.531	0.0161	Morse
7.99 × 1.35	0.535	0.0161	Morse
7.99 × 2.63	0.520	0.0160	Morse

the terms b_1 have values similar to the zero order terms of the linear fit of Eq. (12).

Table 2 shows the values of the identified flexural modulus E_f and shear modulus G_{LJ} for the different bilayer graphenes simulated. All the mechanical stiffness values are increased when the Morse potential is adopted, rather than the AMBER one. This characteristic can be explained by the higher stretching constant k_r in the linearised Morse model. The flexural modulus E_f ranges between 0.371 TPa for the AMBER model, to 0.531 TPa for the linearised Morse potential. These values are very close to the 0.5 TPa measured by Frank et al. in suspended multilayer graphene with AFM techniques [7]. The equivalent transverse shear offered by the LJ potential during the bending deformation is very low, ranging between 14.2 GPa for the AMBER model to the 16.1 GPa for the Morse potential. It appears that the bilayer graphene deforms similarly to a sandwich structure with a relatively stiff core. For a sandwich beam, the condition parameter for a weak core is $(E_f/E_{LJ})/(t\bar{h}^3/h^2)$, which must be higher than 16.7 to completely neglect the bending contribution from the core [12]. We do not have information about a possible equivalent Poisson's ratio of the core, so to obtain the isotropic relation $E_{LJ} = 2G_{LJ}(1+\nu)$. We note that for positive Poisson's ratios $0 < \nu < 0.5$, the weak core parameter would be always lower than 7.25 for the AMBER case and 9.10 for the linearised Morse potential. For $\nu = -0.5$, the shear and Young's modulus would be equal, and the weak core parameter would range between 15.5 and 18.8 – denoting a marginally weak core sandwich. However, from Fig. 3 (and the lack of linear dependence over x^2 above $x/a = 0.2$) it is possible to argue that the core does not contribute to the transverse deformation under pure shear conditions, and the LJ potential provides a complex shear response to the out-of-plane load.

It is interesting, at this point, to consider the membrane stiffness of the single layer sheets connected by the Van der Walls force. Assuming an overall isotropic behaviour and a hinging-stretching deformation mechanism for the covalent bonds, the homogenised Young's modulus for the single layer graphene can be represented by [20]:

Table 3
Tensile membrane stiffness and rigidities for the graphene layers with the identified thickness (Table 1).

Force model	Thickness [nm]	E_{gs} [TPa]	Y_{gs} [TPa nm]
AMBER	0.111	3.467	0.385
AMBER	0.112	3.380	0.377
AMBER	0.116	3.058	0.355
Morse	0.103	4.375	0.451
Morse	0.106	4.029	0.427
Morse	0.107	3.992	0.420
Morse	0.108	3.819	0.412
Morse	0.109	3.719	0.405

$$E_{gs} = \frac{4\sqrt{3}k_r K_h}{3d(k_r + 3K_h)} \tag{14}$$

Where the hinging constant is $K_h = 8k_\tau/d^2$ [20]. The tensile rigidity Y_{gs} is given by the product between the Young's modulus E_{gs} and the thickness d. The in-plane Young's modulus (14) and tensile rigidities have been computed for the different force models and thickness identified during the energy minimisation process, with the results shown in Table 3. The Young's modulus E_{gs} vary between 3.058 TPa and 4.375 TPa, in good agreement with values found by Huang et al. using first and second generation Tersoff–Brenner potentials (4.27 TPa [35]). A common comparison metrics is the use of the tensile rigidities, because of the inclusion of the thickness in the mechanical term. Our models tend to predict a slightly stiff membrane rigidities (between 0.355 and 0.451 TPa nm). However, those values are in line with the ones from Cho et al. (0.386 TPa nm [15]), Chang and Gao (0.360 TPa nm [32]), Sakhaee-Pour (0.354 TPa nm [38]) and Kudin et al. (0.345 TPa nm [37]). The tensile rigidity on circular single layer graphene sheets subjected to pretension and loaded with a point force has been measured equal to 0.335 TPa nm [11].

4. Conclusions

We have shown that the transverse mechanical deformation of bilayer graphene can be approximated by a first order shear deformation theory mutated from the analysis of structural sandwich beams and panels. Using this approach, it is possible to identify the separate contributions given by the single graphene layers and the LJ interlayer potential to the flexural modulus and transverse shear of the nanostructure. Through the minimisation of the total potential energy, we identify different thicknesses of the single graphene sheets composing the bilayer, the thicker graphene corresponding to the mechanically loaded sheet. In that sense, the bilayer graphene behaves mechanically as a nonsymmetric sandwich structure. The present first order theory seems to identify with a good accuracy the flexural modulus of the graphene sheets. The bilayer models represented with the atomistic-continuum technique provide an overall transverse pure shear behaviour in sections of the bilayer close to the supports, while the LJ potential seems to generate a more complex shear behaviour close to the mid-span of the bilayer graphene, suggesting that higher order shear and bending deformation sandwich theories could be developed, with specific emphasis on bilayer and multilayer graphene systems. Nevertheless, the FOSS approach could provide the basis for a post-processing of experimental results carried out on bilayer graphene, instead of using continuum mechanics force displacement models based on single layer systems.

Another novelty of this work is the establishment of a atomistic-continuum FE technique for the C–C bonds of the graphene and the equivalent mechanical nonlinear springs simulating the LJ potential. This simulation approach allows to reproduce a full scale

mechanical testing of the bilayer nanostructure with different loading and boundary conditions.

Acknowledgements

F.S. acknowledges the logistic support of the FP6-NMP-2003-STRP-01364 CHISMACOMB Project for the CPU time. S.A. gratefully acknowledges the support of the Leverhulme Trust for the award of the Philip Leverhulme Prize. R.C. acknowledges the support of Royal Society through the award of the Newton International Fellowship.

References

[1] J.B. Oostinga, H.B. Heersche, X. Liu, A.F. Morpurgo, L.M.K. Vardersypen, Nat. Mater. 7 (2007) 151.
[2] E.V. Castro, N.M.R. Peres, J.M.B. Lopes Dos Santos, F. Guinea, A.H. Castro Neto, J. Phys.: Conf. Ser. 129 (2008) 012002.
[3] H. Hibino, S. Mizuno, H. Kageshima, M. Nagase, H. Yamaguchi, Phys. Rev. B 80 (2009) 085406.
[4] A.N. Pal, A. Ghosh, Appl. Phys. Lett. 95 (2009).
[5] A.N. Pal, A. Ghosh, Phys. Rev. Lett. 102 (2009).
[6] J.C. Meyer, A.K. Geim, M.I. Katsnelson, K.S. Novoselov, D. Obergfell, S. Roth, C. Girit, A. Zettl, Solid State Commun. 143 (2007) 101.
[7] I.W. Frank, D.M. Tanenbaum, A.M. van der Zande, P.L. McEuen, J. Vac. Sci. Technol. B 25 (2007) 2558.
[8] A. Hemmasizadeh, M. Mahzoon, E. Hadi, Thin Solids Films 416 (2008) 7636.
[9] A.K. Geim, K.S. Novoselov, Nat. Mater. (ISSN 1476-1122) 6 (2007) 183.
[10] G.V. Lier, C.V. Alsenoy, V.V. Doren, P. Greelings, Chem. Phys. Lett. 326 (2000) 181.
[11] C. Lee, X. Wei, J.W. Kysar, J. Hone, Science 321 (2008) 385.
[12] H.G. Allen, Analysis and Design of Structural Sandwich Panels, Pergamon Press, Oxford, 1969.
[13] A.P.P. Nicholson, D.J. Bacon, J. Phys. C (1977).
[14] P.P. Gillis, Carbon 22 (1984) 387.
[15] J. Cho, J.J. Luo, I.M. Daniel, Compos. Sci. Technol. 67 (2007) 2399.
[16] J.L. Tsai, J.F. Tu, Mater. Design 31 (2010) 194.
[17] S. Kitipornchai, X.Q. He, K.M. Liew, Phys. Rev. B 72 (075443) (2005) 1.
[18] H. Shen, V.S. Sokolinsky, S.R. Nutt, Compos. Struct. (2004) 115.
[19] F. Scarpa, S. Adhikari, J. Phys. D: Appl. Phys. 41 (2008) 1.
[20] F. Scarpa, S. Adhikari, A.S. Phani, Nanotechnology 20 (2009) 065709.
[21] O.A. Shenderova, V.V. Zhirnov, D.W. Brenner, Crit. Rev. Solid State Mater. Sci. 27 (2002) 227.
[22] C.D. Reddy, S. Rajendran, K.M. Liew, Nanotechnology 17 (2006) 864.
[23] C.Q. Sun, Y. Sun, Y.G. Nie, Y. Wang, J.S. Pan, G. Ouyang, L.K. Pan, Z. Sun, J. Phys. Chem. C 113 (2009) 16464.
[24] L.A. Girifalco, M. Hodak, R.S. Lee, Phys. Rev. B 62 (2000) 13104.
[25] S. Timoshenko, Theory of Plates and Shells, McGraw–Hill, Inc., London, 1940.
[26] T. Kaneko, J. Phys. D: Appl. Phys. 8 (1974) 1927.
[27] W.D. Cornell, et al., J. Am. Chem. Soc. 117 (1995) 5179.
[28] J.S. Przemienicki, Theory of Matrix Structural Analysis, McGraw–Hill, New York, 1968.
[29] ANSYS REL. 11 User's Manual, ANSYS Inc., Canonsburg, PA, 2008.
[30] M. Schwartzbart, A. Steindl, H. Troger, Proc. Appl. Math. Mech. 8 (2008) 10343.
[31] E.J. Duplock, M. Scheffler, P.J.D. Lindan, Phys. Rev. Lett. 92 (2004) 225502.
[32] T. Chang, H. Gao, J. Mech. Phys. Solids 51 (2003) 1059.
[33] C.Q. Sun, H.L. Bai, B.K. Tai, S. Li, E.Y. Jiang, J. Phys. Chem. B 107 (2003) 7544.
[34] R.C. Batra, S.S. Gupta, J. Appl. Mech. 75 (2008) 0601010.
[35] Y. Huang, J. Wu, K.C. Hwang, Phys. Rev. B 74 (2006) 245413.
[36] Z. Tu, Z. Ou-Yang, Phys. Rev. B 65 (2002) 233407.
[37] K.N. Kudin, G.E. Scuseria, B.I. Yakobson, Phys. Rev. B 64 (2001) 235406.
[38] A. Sakhaee-Pour, M.T. Ahmadian, A. Vafai, Solid State Commun. 147 (2008) 336.